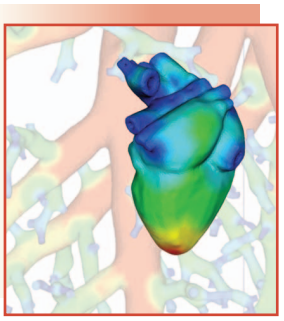

© Images courtesy of Daniel Einstein

Computational Fluid Dynamics

Multiscale Simulation of Gas Flow in Subject-Specific Models of the Human Lung

BY CHING-LONG LIN, MERRYN H. TAWHAI, GEOFFREY McLENNAN, AND ERIC A. HOFFMAN

Variation in the individual airway geometry makes subject-specific models essential for the study of pulmonary air flow and drug delivery. Recent evidence also suggests that early exposure to environmental pollutants has chronic, adverse effects on lung development in children from the age of ten to 18 years [1]. Thus, the capability of predicting air flow and particle deposition in the subject-specific breathing lungs is highly desirable for understanding the correlation between structure and function and for assessing individual differences in vulnerability to airborne pollutants. Furthermore, it has been demonstrated that a strong interaction exists between lung geometry and gas properties [2]. The interaction has major implications in determining gas delivery to and clearance from the lung periphery during ventilation imaging through X-ray computed tomography (CT) using xenon gas [3]–[5] or magnetic resonance imaging (MRI) using hyperpolarized helium gas [6]–[9]. Although there is a critical need to understand these geometry–property interactions, the current state of knowledge acquired from experiments is still far from revealing the true nature of their interplays. At the same time, three-dimensional (3-D) computational fluid dynamics (CFD) simulation of air flow for the entire lung geometry remains intractable because of constraints on imaging resolution and computational power. As a result, current 3-D CFD simulations of air flow are often restricted to a few generations of branching on a fixed mesh, and most studies are based on idealized Weibel airway models. With advances in imaging and computing technologies, anatomy coupled with functional measures (ventilation and perfusion) can now be obtained via CT imaging [10], [11]. These measures provide the detail needed to interrogate the utility of CFD in providing insights into subject-specific differences in regional lung function and the underlying mechanisms of pathologic developments.

In this article, we describe a comprehensive CFD framework for pulmonary gas flow that 1) utilizes subject-specific airway geometries, 2) spans multiple scales from largest bronchial airways to terminal bronchioles, and 3) employs a novel CT-data-driven approach to simulate flow in a breathing lung. Modeling flow in a subject-specific breathing lung is an extremely challenging task because of the complexity of lung geometry, which is dynamic in time and multistage in nature. A further challenge is the necessity of using advanced CFD techniques and large-scale high-performance parallel computing to achieve multiscale simulation in a moving airway–wall setting and resolving turbulent flow and its transition to laminar flow. Development of such a model can only be accomplished through multidisciplinary efforts that require expertise in medical imaging, airway geometric reconstruction, computational techniques, pulmonary physiology and medicine, and fluid mechanics. We will present the newly emerging techniques developed in a collaborative effort for 1) CT image acquisition and segmentation, 2) multiscale 3-D and one-dimensional (1-D) coupled mesh generation, 3) 3-D and 1-D CFD techniques with the large-eddy simulation (LES) capability for high Reynolds number turbulent flow in the upper airways, 4) the CT-derived subject-specific physiologically realistic boundary conditions for CFD, 5) the fluid-structure interaction (FSI) algorithm for regional interplay between flow and tissue, and 6) the simulation strategy for low Reynolds number acinar flow.

The capability of this novel computational framework will bring about a new understanding of the relationship between structure and function in pulmonary air flow; we can now study this relationship in subject-specific breathing lungs. The applications of the model include, but are not limited to improving pharmaceutical aerosol drug delivery (there is a growing interest in delivering drugs via inhalation, such as insulin, growth hormone, etc.); predicting subject-specific regional ventilation for study of progression of lung diseases; designing subject-specific protocols for CT and MRI through specific gas mixture compositions; and predicting long-term effects of environmental pollutants on lung function.

Methodologies

This section describes the five major components in developing a high-fidelity, subject-specific computational framework: CT image acquisition and analysis, geometric modeling of airway trees, 3-D and 1-D coupled mesh generation, 3-D and 1-D CFD techniques, and CT-derived physiological boundary conditions for CFD simulations.

Digital Object Identifier 10.1109/MEMB.2009.932480

Variation in the individual airway geometry makes subject-specific models essential for the study of pulmonary air flow and drug delivery.

Multidetector-Row CT Image Acquisition and Segmentation

The multidetector-row CT (MDCT) imaging procedures were approved by the University of Iowa Institutional Review Board. CT data were acquired at the Iowa Comprehensive Lung Imaging Center (I-CLIC), the University of Iowa, by use of a Siemens Sensation 64 MDCT scanner. Scan parameters are as follows: 120 kV, 100 mA·s, pitch 1.2, slice width 0.6 mm, slice interval 0.6 mm. Images consist of a spiral scan of the full lung, with the inflation level held at 95% vital capacity to resolve as many generations of airways as possible. Subjects are imaged supine. The MDCT images are processed using an in-house derived software package dubbed the Pulmonary Workstation plus (PW+) to segment the lungs, lobes, and intrathoracic as well as upper airways [12]. PW+ airway segmentation is based on a combination of 3-D region growing and two-dimensional (2-D) mathematical morphology methods. The software has been demonstrated to successfully extract airway trees from most clinical quality standard-dose MDCT data. Figure 1 illustrates the major functions of PW+. Figure 1(a) shows the 3-D CT-segmented airway tree (blue and brown) and the 3-D vessel tree (cyan) derived from the CT image data. Figure 1(b) displays the coronal view of the CT data, cutting through the trachea and the main-stem bronchi. The gray level of each voxel can be used to determine the air content in the lung tissue. Figure 1(c) shows a virtual flythrough of the airway lumen in the trachea having ring-like structures toward the first bifurcation. A path of the segmented airways can be selected and highlighted by the blue color as shown in Figure 1(a), and its axial cross-sectional view of the airways can be displayed and analyzed as shown in Figure 1(d). The airway walls are the regions between the two red solid lines on both sides of the airway lumen in the image, and the distance between them is the airway

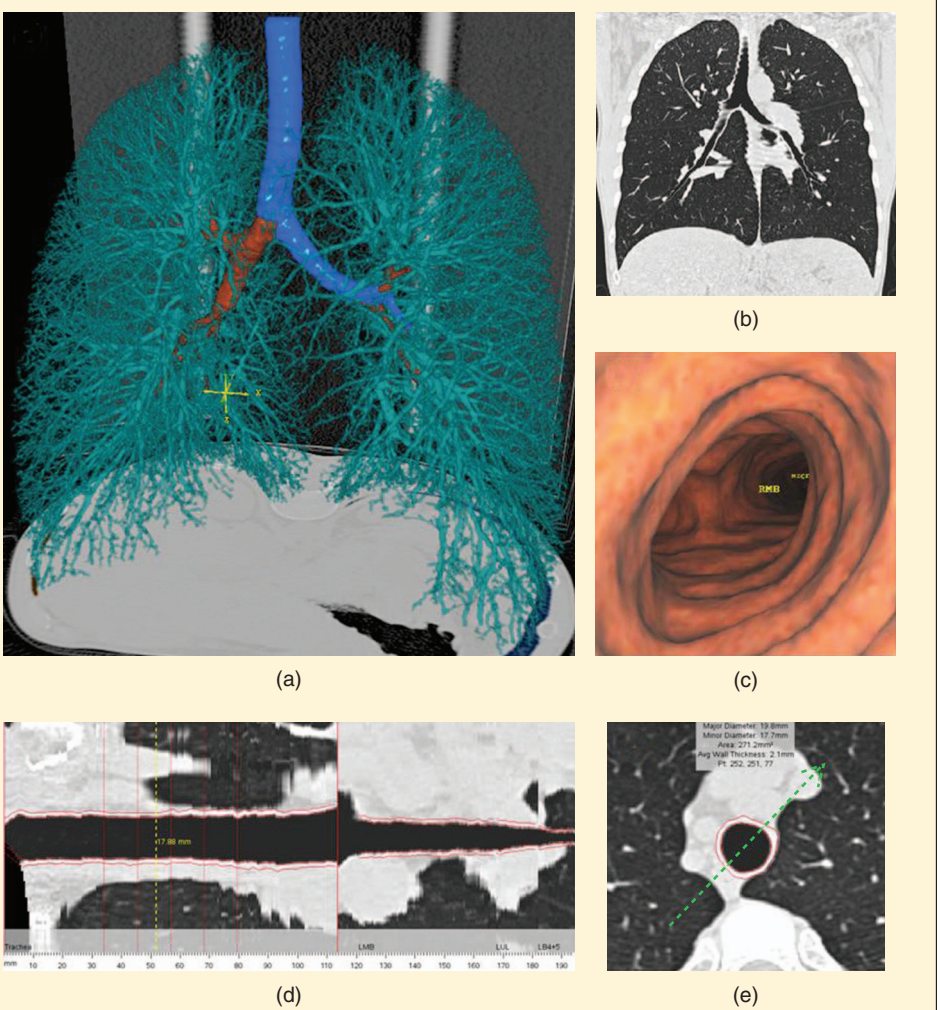

Fig. 1. (a) 3-D surface rendering of airway (blue and brown) and vessel (cyan) trees of a human subject, (b) coronal view of CT data, showing the trachea, the main-stem bronchi, and the lung tissue, (c) virtual flythrough of the trachea facing the first bifurcation (right main-stem bronchus (RMB)), (d) axial cross-sectional view along the blue color-coded airways in (a), which is chosen arbitrarily, and (e) perpendicular view of the airway along the yellow dashed line in (d).

Modeling flow in a subject-specific breathing lung is an extremely challenging task.

wall thickness. The perpendicular view at any location along the selected path can also be displayed as illustrated in Figure 1(e), showing the major and minor diameters of the airway at that specific region. The airway tree obtained by our segmentation method is skeletonized to identify the centerlines of individual branches and branch-point locations. Centerlines and associated airway structures are labeled, and the volume and surface area of each segment are determined. The PW+ also automatically exports the segmented airway surface geometry to a stereolithography (STL) file, which can be further used for generating CFD meshes via the conventional methodology or for building physical solid models via the rapid prototype processing.

Geometrical Modeling of Airway Trees

Methods for deriving centerline models of the entire airway tree from CT imaging are now well established. We have previously presented methods to derive a geometrical model for the airway tree that spans the entire conducting airway system from trachea to terminal bronchioles [13]. The airway tree model incorporates anatomical geometric data for the imaged and segmented airways and the shape of the lungs and lobes, and a branching algorithm to grow the entire airway tree. The algorithm uses the centerlines of the imaged airways as the initial condition and the shape of the imaged lung/lobes as the boundary condition to generate a subject-specific model. To date, this is the only published method that has been demonstrated to produce models of the airway tree that have geometry consistent with the morphometric measurements in human and animal (sheep). The resulting model is a 1-D centerline tree, with the branches distributed in 3-D space. To use the model for computation, diameters must be defined through the entire structure. To date, computational studies using this model have assumed circular cross sections for the airways [14], [15]. For the imaging-based (uppermost) airways, the diameters are assigned directly from calculating the diameter based on the measurement of airway cross-sectional area in a plane orthogonal to the central axis. The algorithm-based airways can have diameters assigned using Horsfield or Strahler ordering [13] weighted against a ratio to parent branch diameter. Figure 2(a) and (b) shows a 1-D human airway model at total lung capacity (TLC), overlaid with geometry fitted 2-D surfaces for the uppermost airways. In Figure 2(a), the diameters of the 1-D airways are rendered, whereas in Figure 2(b) only the centerline locations of the 1-D mesh are shown.

3-D and 1-D Coupled Mesh Generation

The physiologically consistent spatial distribution of airways in our 1-D tree structure is essential in bridging scales to predict regional ventilation. However, for computing 3-D flow and pressure, we require a 3-D structure that incorporates the salient features of the airway geometry. Previous models of the airway tree have simplified the computation domain by representing the airways as smooth cylinders or have considered only a few of the up to 30 generations in the conducting airway tree. The reason for this is clear: constructing a CFD-appropriate computational mesh of the airways is complex and time consuming, and imaging data for the lower airways is generally not attainable.

We have developed a new method to construct subject-specific 3-D and 1-D coupled airway mesh structures that allow us to move seamlessly between scales, incorporating the desired level of geometric detail at any region of interest in the

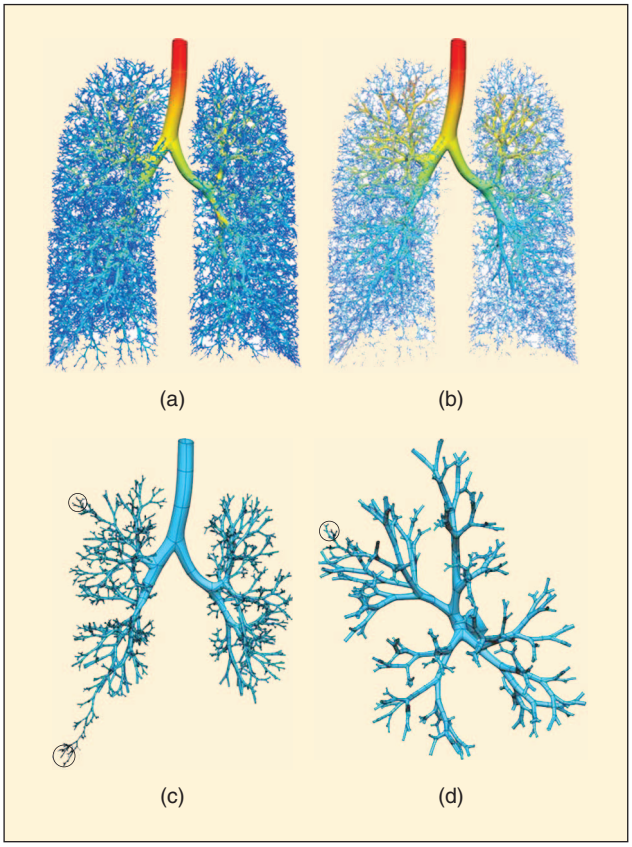

Fig. 2. Multiscale anatomically based meshes of the airway tree in a single subject. (a) 1-D volume-filling tree with rendered airway diameters, (b) 1-D airway tree centerlines and 2-D surface mesh for all airways, (c) 2-D surface mesh in (b) that starts from the trachea to generation 11, and a path in each of the right upper and right lower lobes that extend to the terminal bronchioles up to 28 generations inside the circles, and (d) the right upper lobe surface mesh for airways to generation 11 and one longer pathway inside the circle.

Free-form deformation is a relatively low-cost method to define volume change on an anatomical basis.

tree. The method is underpinned by the subject-specific anatomically based 1-D centerline models for the entire conducting airway tree. We start by converting the 1-D tree to a high-order (cubic Hermite) 2-D surface mesh of the entire domain, where the airway surface is discretized circumferentially and axially. This is achieved by defining a generic bifurcation that is scaled, translated, and rotated automatically to match the position and size of each bifurcation in the 1-D tree. At the bifurcations, the parent and child branches merge with a smooth, continuous surface as shown in Figure 2(c) and (d). The 2-D surface mesh uses high-order elements to represent surface curvature and derivative continuity efficiently.

To capture the subject-specific geometric features of the imaged airways, the 2-D surface mesh of the uppermost airways is geometry fitted to data for the inner surface of the airway wall extracted from volumetric imaging. Geometry fitting can include smoothing, and so we can manipulate the data fit to smooth out noisy data or fine-scale anatomical features, or the smoothing can be relaxed to allow inclusion of geometric detail. The resulting 2-D surface mesh not only has anatomical detail for the direction and surface geometry of the imaging-based upper airways but also is continuous with the surface of the algorithm-based lower airways. This is because the circular diameters of the lower airways were assigned such that they had a morphometrically consistent relationship with the uppermost (imaged) airways.

Any portion of this surface mesh can be converted to a 3-D CFD-ready mesh. In our method, we select a region of interest that we would like to study in detail, for example, all airways to a specified generation or along a specified path, as shown in Figure 2(c) for the trachea to all-generation 11 branches, plus two pathways to the terminal bronchioles (28 generations). The 3-D mesh is then created within those airways only, and for computation, the remainder of the domain is the original 1-D tree. This approach means that we are not restricted to studying only a specific region or level of airway. Importantly, the 3-D and 1-D models are not separate structures that are artificially joined together: they are a single model that merely has a different dimension in specified regions. This gives us unparalleled flexibility in choosing the region that we wish to study with detailed computation. The multiscale nature of our meshing methodology is illustrated in the sequence of images in Figures 2 and 3. The volume-filling 1-D mesh is shown in Figure 2(a) and (b), and the 2-D mesh of a selected domain in Figure 2(b) and (c). Figure 2(d) shows the 2-D surface mesh of the right upper lobe in this model, and Figure 3(a) and (b) overlays a portion of the tetrahedral volume mesh to illustrate its consistency with the lower dimension meshes.

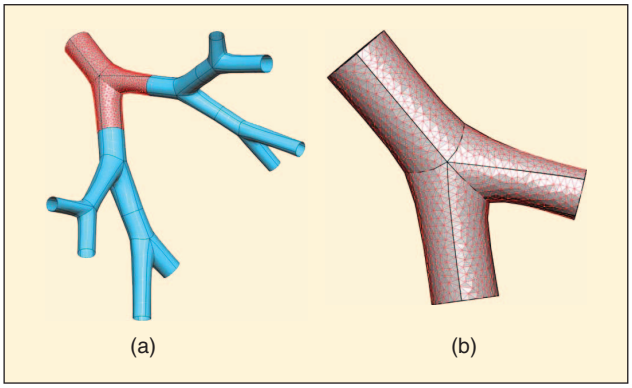

Fig. 3. (a) A subset of the right upper lobe mesh, overlaid with a 3-D tetrahedral volume mesh for a bifurcation unit, and (b) the tetrahedral mesh for the bifurcation unit in (a).

We currently use the open source software Gmsh (www.geuz.org/gmsh) to generate tetrahedral meshes within subdomains throughout the airway tree. Gmsh uses a description of a domain boundary surface and fills this with an unstructured mesh. The approach is therefore similar to the conventional method of exporting STL files that represent anatomical surfaces from volumetric imaging and volume filling the structure with a tetrahedralized CFD mesh [16]–[18]. However, our intermediate step of creating a high-order 2-D surface mesh means that we can merge the imaged airway domain with the algorithm-based domain without a discernable difference in the topology of the mesh: using STL (or similar) surface geometry descriptions for the airways cannot seamlessly couple imaging with representations of more distal branches in this way. The conventional approach to mesh generation is to follow the surface domain description with volumetric meshing of the entire domain as a single structure, or arbitrarily and manually dividing the domain into smaller meshing units for convenience. As a consequence of the systematic structure of our surface mesh, we automatically divide the domain into many small volume meshing subunits for parallel computation. We have developed a software that is external to Gmsh to control volume filling of sequential subunits, to check consistency between adjacent subunits, and to convert the final structure to our preferred format for computation.

A major advantage of our approach is that we can study transport in a ten-generation 3-D-meshed model, for example, successively include additional generations in the 3-D-meshed portion of the model to evaluate the influence of additional generations, and to define the conditions under which a 1-D model representation will suffice. Three-dimensional equations are solved in the CFD-ready zone, coupled with equations for 1-D flow in the 1-D airway zone, resulting in a truly multiscale model.

CFD Techniques

Both 3-D and 1-D CFD techniques are used for multiscale simulations. For 3-D flow simulation, the custom-developed,

The coupled FSI system is treated as a triple-domain problem that includes the fluid domain, the structure domain, and the moving mesh.

characteristic Galerkin finite element method is applied to solve 3-D incompressible, variable-density Navier–Stokes equations [19]. A fractional four-step projection method is employed to enforce mass conservation. To model a breathing lung with compliant airways and moving mesh, the arbitrary-Lagrangian–Eulerian (ALE) method has been implemented into the 3-D model. For capturing turbulent flow, the high-fidelity LES technique is adopted. The current LES with a Vreman subgrid scale model [20] has been validated and verified by several benchmark cases, such as turbulent channel flow, that accurately captures the law-of-the-wall mean velocity profile [18]. The 3-D CFD model is of second-order accuracy in both time and space and has been fully parallelized using message-passing interface (MPI) for large-scale, high-performance parallel computation. The 1-D flow model is based upon the integral form of continuity and energy equations, i.e., the pressure-flow-resistance approach [21].

Physiologically Realistic Boundary Conditions

Traditional boundary conditions for airway CFD studies prescribe either pressure or flow at the domain outlets, often setting them to be identical at each outlet for simplicity. In reality, the distribution of ventilation is regionally dependent and driven by expansion of the nonlinearly elastic, compressible lung tissue. To prescribe subject-specific and physiologically realistic boundary conditions, we have been developing three methods that use (in the order of increasing complexity) 1) gray levels in CT images, 2) free-form deformation [22], and 3) models for the soft tissue deformation of the lung [21] to define the peripheral tissue volume change and therefore prescribe regionally varying, and physiologically appropriate, boundary conditions.

In the first image-based method, the air content can be calculated for each voxel at both TLC and functional residual capacity (FRC) from the gray level of the CT images (assuming only lung tissue, blood, and air in the voxel). The flow rate at each of the terminal bronchioles can then be computed using the time rate of change of air volumes between TLC and FRC in the units of two lungs, or five lobes, or parenchymal units surrounding terminal bronchioles. By mass conservation, the flow rates at the exit faces of the 3-D airway model can be determined by summing the flow rates at the terminal bronchioles using the connectivity information (that is embedded in the 3-D and 1-D coupled mesh) between the 3-D airway exit faces and the associated downstream 1-D airway branches.

In the second free-form deformation method, an affine transformation of a host mesh is computed to control the shape change of a structure that is embedded within the host. In our case, we embed a finite element mesh of the lung at TLC and use a small number of anatomical control points to compute the transformation to FRC. The transformation tensor can also be used to calculate the change in location and size of the airways, whether in a 1-D, 2-D, or 3-D CFD-ready form. The terminal bronchioles in our model airway trees are each associated with a specific region of tissue, representing a pulmonary acinus. The transformation from TLC to FRC results in a regional, nonuniform volume change that we assume is equivalent to air flow from the peripheral tissue. The local peripheral tissue volume change in a specified time interval is set as a flow boundary condition at the corresponding terminal bronchiole. The connectivity of our multiscale 3-D and 1-D model ensures that the boundary conditions are propagated appropriately up the airway tree. Free-form deformation is a relatively low-cost method to define volume change on an anatomical basis.

In the third soft tissue mechanics-based method, we have developed a model for the large, nonuniform, elastic deformation of the compressible lung–air system [21]. This model is used to calculate local expanding pressures that act on the airways and the local volume change of the peripheral tissue for setting flow boundary conditions as in the free-form deformation method. The model requires definition of its material properties, the direction and magnitude of gravity, and the restriction of lung shape to mimic the constraint of a diaphragm and chest wall. In the model, the lung is free to slide, and the compressible mesh elements can change in volume. Finite deformation elasticity is used to compute stress and strain; therefore, the model is appropriate for large strains. By using this model to define the boundary conditions in our coupled airway mesh, we can study gas transport as well as tissue mechanics at different lung volumes in different orientations.

Results

This study primarily considers pulmonary air flow. For mixing of air with inert gases, please refer to [16]. The air properties used here are a density of 1.2 kg/m^3 and a kinematic viscosity of 1.7×10^{-5} m^2/s.

Effect of Upper Large Airways

We have applied the LES technique to the CT-based human airway models to address two important issues in CFD studies of air flow: 1) the effect of a realistic geometry that reflects the detail of the in vivo human airway and 2) the characteristics of the turbulent laryngeal jet and its effect on air flow in the intrathoracic airways [18]. To understand the relative importance of the upper and intrathoracic airways and their role in determining central air flow patterns, we create two geometries from MDCT data of human subject H869. In addition to CT data, the gender, ethnicity, and pulmonary function test data of the subject are archived with a subject identification number in our medical image file archive system. Thus, the number H869 is provided for reference by other researchers who would like to further analyze this subject. The first geometry consists of a mouth piece, the mouth, the oropharynx, the

larynx, and the intrathoracic airways of up to six generations. The second geometry comprises only the intrathoracic airways (the upper airways are referred to as those in the first geometry, excluding the intrathoracic airways). Both LES and direct numerical simulation (DNS) techniques have been applied to resolve turbulence. A uniform velocity boundary condition is imposed at all of the exit faces of the terminal branches to generate a constant inspiratory flow rate of 320 mL/s, resulting in a mean speed of 2 m/s and a Reynolds number of 1,700 in the trachea. In the first geometry case, a curved sheet-like turbulent laryngeal jet is formed and impinges on the rear side of the trachea with high turbulence intensity in the subglottic space and the upper trachea. In contrast, the velocity distribution in the second geometry case is a parabola, with its maximum located along the centerline of the trachea and the turbulence intensity is essentially zero, and thus the flow is laminar. The velocity characteristics in the left and right main-stem bronchi between the two cases are also different. The presence of turbulence is found to increase the maximum localized wall shear stress threefold in comparison to the second geometry case [18].

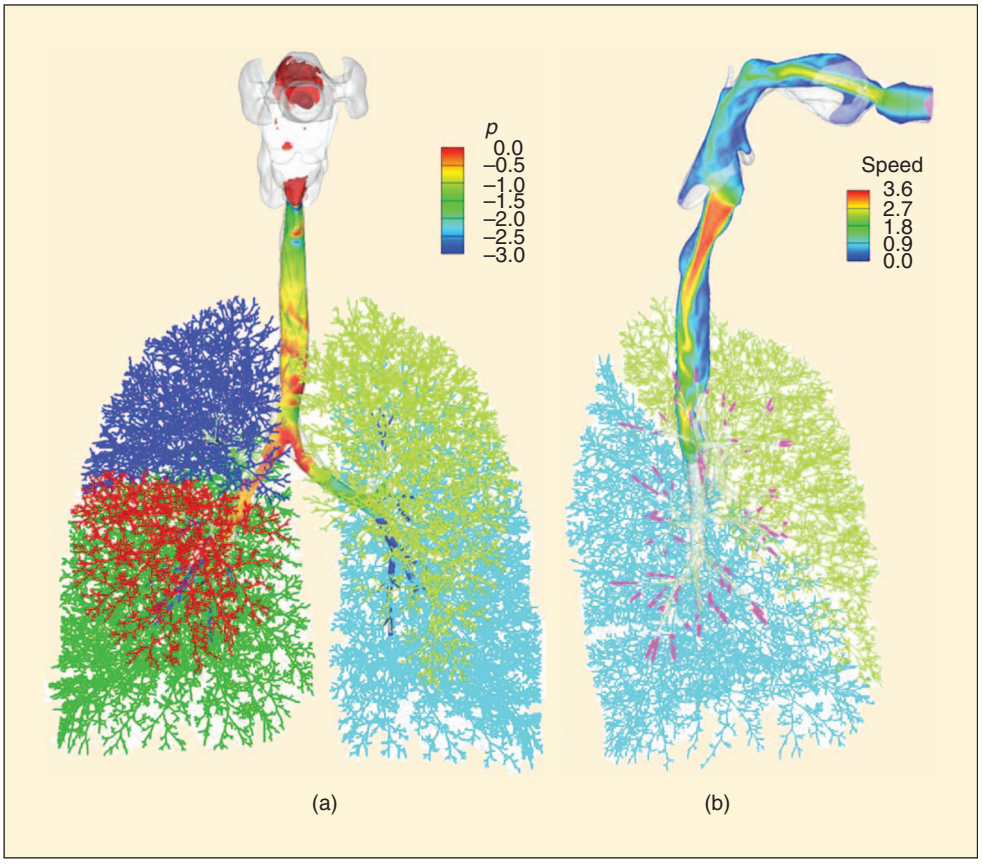

Fig. 4. (a) 3-D CT-resolved airways and 1-D airways in each of the five lobes with different colors (front view). The laryngeal jet at peak inspiration is revealed by the isosurface of the air speed at 1.5 m/s. The jet is color coded by the pressure (p) contours (unit, Pa). (b) The contours of the air speed (unit, m/s) in a vertical plane together with the 1-D airways in the left upper lobe and the left lower lobe (side view). The velocity vectors at the boundary faces of the model are displayed in pink.

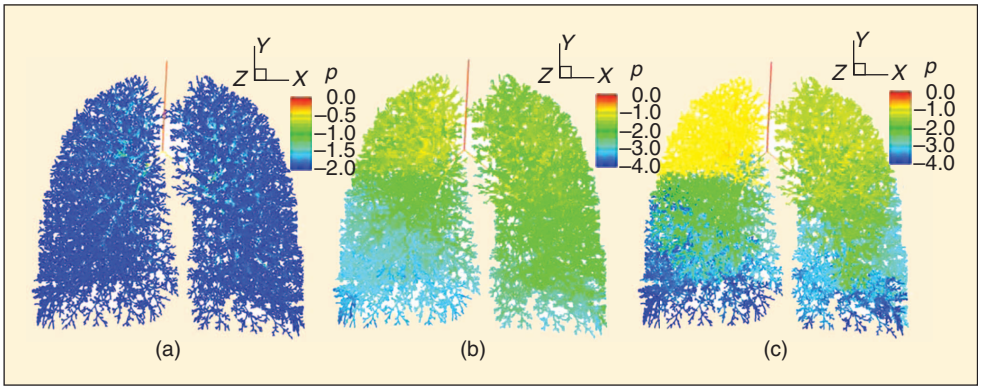

Fig. 5. Pressure contours of air flow in a subject-specific airway tree model, with the boundary condition of (a) uniform pressure, (b) uniform flow, and (c) regional ventilation based upon lobar air volume changes.

To assess intersubject variability and boundary-condition effect, we have applied the LES in 3-D/1-D meshes together with a pulsatile breathing waveform and the aforementioned image-based boundary condition to a different human subject H644. Because the scanning protocol used for H644 differs from that of H869, the CT data for H644 does not contain the upper airways. Thus, the upper airway geometry of H869 is used to produce the laryngeal jet. Figure 4 shows the 3-D CT-resolved airway geometry together with the 1-D airway tree of the same subject. The 3-D CT-resolved airway geometry consists of 899,465 nodes and 4,644,447 tetrahedral elements, and the 1-D tree consists of 63,345 nodes and 63,344 line elements. The entire 3-D mesh is partitioned into 256 parts, and the CFD simulation has been carried out on TeraGrid clusters using 256 CPU cores. The breathing waveform has a time period of 4.8 s and produces a tidal volume of 500 mL. At peak inspiration, the mean speed in the trachea is 1.24 m/s, and the corresponding Reynolds number based on the mean speed and the average diameter of the trachea is 1,364. With the use of physiologically realistic boundary condition via the

subject-specific CT gray-level number and 1-D airway model, the partition of air flowing into the five lobes is (left upper lobe, left lower lobe, right upper lobe, right middle lobe, right lower lobe) = (0.1447, 0.3489, 0.1296, 0.0522, 0.3246), and the ratio of air volume flowing into the left and right lungs is 0.975; i.e., the ventilation of each of the five lobes and each of the two lungs in the CFD simulation is determined by individualized CT data. This is an important feature for study of heterogeneity in regional lung function. The 3-D structure of the laryngeal jet at peak inspiration is revealed in Figure 4(a) by the isosurface of the air speed, which is color coded by the pressure. Figure 4(b) shows the cross-sectional view of the unsteady laryngeal jet that propagates along the trachea downstream into the lung. The jet-induced tracheal wall shear stress may have pathophysiologic implications for reactive inflammation and fibrosis [18]. The flow at the exits of the CT-resolved terminal branches becomes laminar, and the velocity profile is a parabola. It is noted that, without including the upper airways in the CFD simulation, the flow in the trachea becomes laminar and the associated velocity profile is a parabola like the second geometry case of subject H869.

The results suggest the necessity of using the subject-specific 3-D and 1-D coupled mesh and CFD LES analysis to better understand variations in flow characteristics that might contribute to the progression of lung diseases and the response of the lung to inhaled drug aerosols or air pollutants.

Effect of Peripheral Small Airways

To demonstrate the sensitivity and dependence of regional ventilation on boundary conditions, we have applied the 1-D flow model to a 1-D airway tree model with three different boundary conditions. Cases 1 and 2 apply the respective pressure and flow boundary conditions at all of the terminal bronchioles. For case 3, the regional ventilation data are estimated from the image-derived boundary condition based on the variation of air volumes in each of the five lobes at TLC and FRC. Thus, the solution of case 3 can be treated as the most accurate, and it serves as a reference for the other two cases. Figure 5 shows the pressure contours of the three cases, clearly demonstrating the dependence of pressure distribution (and regional ventilation) on boundary conditions. Case 3 is the most physiological, having larger pressure drop in the lower lobes. An immediate conclusion is that the flow rate and pressure specified at the exit faces of the 3-D terminal airways with a limited number of generations may lead to various distributions of regional ventilation in lung parenchyma at a local level, and some may not be physiologically realistic. Thus, the 1-D model serves as a link between 3-D truncated airways and lung parenchyma to determine appropriate flow rates at the 3-D terminal branches, leading to subject-specific ventilation at lobar or regional levels.

Fluid-Structure Interaction

To study the interaction between air flow and airway wall at a local level, its effects on wall shear stress, and its implications for airway remodeling and abnormalities, we have developed a FSI technique based on the aforementioned CFD method [23]. The FSI technique has been integrated with a finite volume-based structural dynamics method as well as a finite element-based structural dynamics method together with a dynamic level-set meshing algorithm. The finite element structural dynamics method accepts brick and tetrahedron elements for finite-walled structures and shell elements for thin-walled structures like alveoli.

The coupled FSI system is treated as a triple-domain problem that includes the fluid domain, the structure domain, and the moving mesh. The governing equations for both domains are solved in an iterative manner: the Navier–Stokes equations are solved first for the fluid domain. The solutions of the fluid provide external forces, including fluid pressure and shear stress to the structure domain. The dynamics equation is then solved for the structure under the influence of fluid forces, which provides deformation and velocity boundary conditions at the fluid-structure interface. The fluid mesh is moved by the dynamic mesh algorithm in accordance with these boundary conditions, which updates the mesh deformation and ALE velocity for the computation of fluid domain for the next time step. The FSI solver has been applied to several FSI problems, such as vortex-induced plate vibration, flow in a 2-D or 3-D flexible tube, flow in an inflating or contracting balloon, and flow in a human bifurcating compliant airway. Figure 6(a) shows the volumetric view of the airway lumen at peak inspiration and resting state at a Reynolds number of 183, which is determined from the CFD solution of [18] at the same site. This corresponds to the flow condition at the airway bifurcation between the third and fourth generations. The bifurcation is assumed to be isotropically tethered to the lung tissue, i.e., a uniform force is exerted on the exterior face of the airway wall. The geometries of the airway lumen and wall of finite thickness are derived from CT data, as illustrated in Figure 1. Figure 6(b) displays the corresponding radial deformation of the airway wall at peak inspiration, showing a relatively large displacement in the direction normal to the plane of bifurcation.

Acinar Flow Simulations

The study of air flow dynamics in the respiratory generations of the human lung (beyond the transitional bronchioles) is important for understanding particle transport and provides rich information on deposition sites for particles (e.g., aerosols) of varying sizes. The two crucial stages in understanding alveolar fluid flow

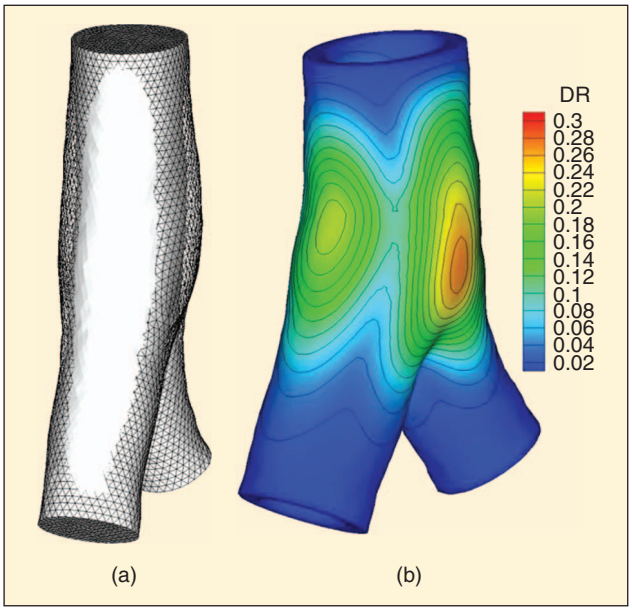

Fig. 6. (a) Volumetric change of the airway lumen between peak inspiration (wireframe) and resting state (gray-shaded surface) at a Reynolds number of 183 and (b) contours of the radial deformation (DR) of the airway wall at peak inspiration.

phenomena are reconstruction of close-to-reality geometry for use in silico and simulation of fluid flow under rhythmic breathing. The calculation of particle transport and deposition follows more easily once the fluid flow data is available.

In the current work, 3-D alveoli are reconstructed and visualized as space-filling polygonal units using a 3-D Voronoi meshing scheme [24]. Figure 7(a) shows that the alveolar opening angles are 90° and 71° in two mutually perpendicular planes. The mouth takes the shape of a noncoplanar hexagon attached to a duct that ventilates fluid uniformly into these cells. Three units share a septa (or common faces) at a dihedral angle of 120°. The central duct is a space formed within this honeycomb with no distinct walls. Figure 7(b) shows an alveolar duct, consisting of 18 alveoli and a central duct. The typical Reynolds number ranges from 1.1 to 0.04. The CFD simulation has been carried out for a breathing period of 2.5 s.

Alveolar flows fall under the category of open cavity flows: these are characterized by interesting features such as stagnation points (under steady conditions, attached to the cavity walls near the corner), recirculation regions, and flow turning around sharp corners. The interaction between the cavity and the duct is inhibited by the presence of diffusion-dominated separatrix or a separation streamline. Even at moderate Reynolds numbers, the presence of unsteadiness in the upstream conditions destroys this streamline. But the absence of inertia at low Reynolds number regimes means that the stagnations points are not destroyed, and instead, they oscillate near the corner. Interestingly, in the presence of wall motion (oscillating normal to itself), a portion of slow-moving fluid close to the duct entrains the cavity, and the recirculation is pushed to one side of the cavity [Figure 7(c)]; this is in agreement with [25].

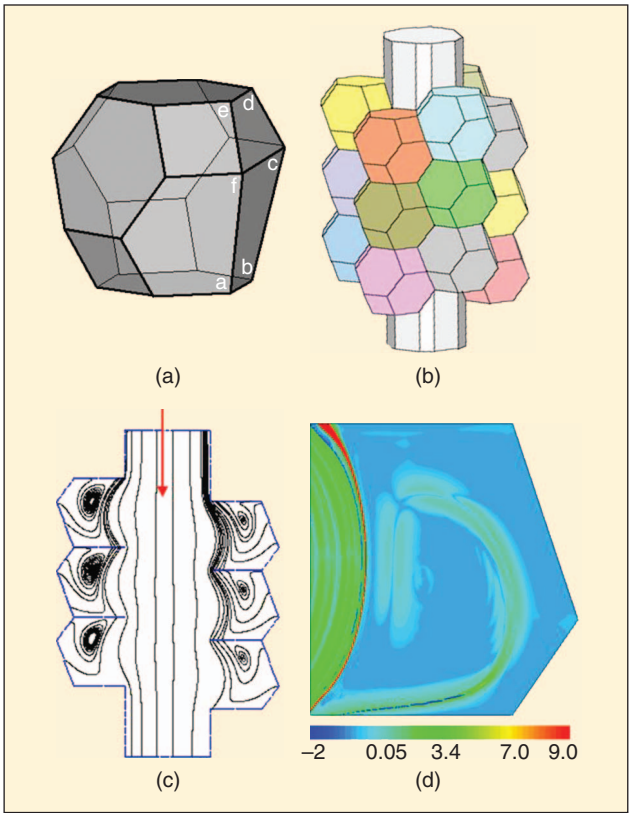

Fig. 7. (a) A typical alveoli unit, where "a-b-c-d-e-f-a" is the entrance, (b) an alveolar duct, (c) streamline at a Reynolds number of 0.5 in a cross section at inspiration (the red arrow denotes the flow direction), and (d) the stretch rate map in the cross section of one of the alveolar sacs in (c).

Streamlines and velocity vectors are not sufficient to reveal the characteristics of unsteady periodic flows. Common methods of visualizing unsteady flows are Poincaré sections, material advection, and stretch rates. Stretch rate calculations, namely, stretching of material lines uniformly distributed in the flow [26], have been performed to quantify the extent of mixing in these low Reynolds number flows. For example, Figure 7(d) shows the stretch rate map. The red contours indicate the regions of high stretch, suggesting that the contribution to mixing from other regions within the cavity is less than the high-stretch regions in a volume-averaged sense.

Conclusions

In this article, we have described a computational framework for multiscale simulation of gas flow in subject-specific airway models of the human lung. The framework consists of five major components: accurate extraction of airway geometry from MDCT image data sets, geometrical modeling of airway trees, novel 3-D and 1-D coupled mesh generation, 3-D high-fidelity CFD techniques for turbulent and transitional flow, and CT-derived subject-specific physiological boundary conditions. This work demonstrates the importance of multiscale simulation of pulmonary gas flow for accurate prediction of flow characteristics at large and small airways and their interactions. The multiscale simulation presented here can be further applied to other healthy and diseased human subjects for intra- and intersubject analyses to better understand the lung flow-structure relationship, the progression of lung diseases, and the correlation between inhaled pharmaceutical drug aerosols or air pollutants with airway structure.

Acknowledgments

The authors would like to thank Edwin van Beek, Guohua Xia, Haegyun Lee, Deokiee Chon, Junfeng Guo, Jiwoong Choi, Haribalan Kumar, Heather Baumhauer, Jered Sieren, and Janice Cook-Granroth for assistance during the course of the study. This work was supported in part by National Institutes of Health (NIH) Bioengineering Research Partnership Grant R01-HL-064368 (Eric A. Hoffman, PI) and an NIH Grant R01-EB-005823 (Ching-Long Lin, PI) awarded through the National Institute for Biomedical Imaging and Bioengineering monitored by Grace Peng under the Interagency Modeling and Analysis Group (IMAG) program for multiscale modeling. The authors also thank the TeraGrid sponsored by the National Science Foundation for allocating the computer time at the National Center for Supercomputing Applications (NCSA) and the Texas Advanced Computing Center (TACC).

Ching-Long Lin received his Ph.D. degree in mechanical engineering from Stanford University in 1994. He joined the University of Iowa in 1997 and is currently a professor in the Department of Mechanical and Industrial Engineering. He is also a faculty research engineer at the Iowa Institute of Hydraulic Research (IIHR)-Hydroscience and Engineering Institute, a member of Applied Mathematical and Computational Sciences Program, and a member of the Environmental Health Sciences Research

Center at the University of Iowa. He received the National Science Foundation Career Award in 1999. His main research interests are turbulence physics, LES, multiscale lung simulation, FSI, four-dimensional data assimilation, lattice Boltzmann method, level-set method for two-phase flow, and high-performance parallel computing.

Merryn H. Tawhai received her Ph.D. degree in engineering science from the University of Auckland in 2001. Since then, she has worked as a consultant to a U.S. biotech company and in the Auckland Bioengineering Institute at the University of Auckland, establishing a research team to develop integrative computational models of the lung for studying pulmonary physiology and pathophysiology. She also holds an adjunct appointment in the Department of Biomedical Engineering at the University of Iowa. Her main research interests are in developing anatomically based finite element models of physical structures in the lung and, using these individualized models to study lung tissue mechanics, ventilation distribution, pulmonary perfusion, airway thermofluid dynamics, and inert gas mixing.

Geoffrey McLennan is a professor of internal medicine, radiology, and biomedical engineering. He is the director of the newly formed Iowa Institute of Biomedical Imaging, the director of the Translational Lung Imaging Research Program, and the director of Interventional Pulmonology. His clinical interests are in general pulmonology and lung cancer, with a particular focus on diagnostic and therapeutic uses of bronchoscopy. His current research is in the development of, and utility of, advanced image acquisition and analysis techniques in the lung. He is also actively involved in developing newer bronchoscopic techniques, especially virtual bronchoscopy, bronchoscopic fluorescence detection, bronchoscopic ultrasound, bronchoscopic confocal microscopy, balloon bronchoplasty, and bronchial stent placement. He has also undertaken clinical research in asthma, lung cancer, and sarcoidosis, and in particular, continues to examine multimodality imaging aspects of lung cancer in National Cancer Institute (NCI)-funded studies.

Eric A. Hoffman received his Ph.D. degree in physiology from the University of Minnesota/Mayo Graduate School of Medicine in 1981. He is a professor of radiology, medicine, and biomedical engineering at the University of Iowa. He is also the director of the Physiological Imaging Laboratory in the Department of Radiology and the director of I-CLIC at the University of Iowa. Throughout his career, he has used advanced imaging methodologies to study basic respiratory physiology centered largely on mechanisms of ventilation and perfusion heterogeneity and regional lung mechanics. Most recently, in addition to continuing basic physiologic research of the lung, he has begun to apply multidetector row spiral CT imaging methodology to objectively follow human lung pathology and pathophysiology, with a particular emphasis on inflammatory lung diseases.

Address for Correspondence: Ching-Long Lin, Department of Mechanical and Industrial Engineering, The University of Iowa, Iowa City, IA 52242. E-mail: ching-long-lin@uiowa.edu.

References

[1] W. J. Gauderman, E. Avol, F. Gilliland, H. Vora, D. Thomas, K. Berhane, R. McConnell, N. Kuenzli, F. Lurmann, E. Rappaport, H. Margolis, D. Bates, and J. Peters, "The effect of air pollution on lung development from 10 to 18 years of age," *New Engl. J. Med.*, vol. 351, no. 11, pp. 1057–1067, 2004.
[2] D. Chon, B. A. Simon, K. C. Beck, H. Shikata, O. I. Saba, C. Won, and E. A. Hoffman, "Differences in regional wash-in and wash-out time constants for xenon-CT ventilation studies," *Respir. Physiol. Neurobiol.*, vol. 148, no. 1–2, pp. 65–83, 2005.
[3] J. K. Tajik, B. Q. Tran, and E. A. Hoffman, "Xenon enhanced CT imaging of local pulmonary ventilation," *Proc. SPIE*, vol. 2709, pp. 40–54, 1996.
[4] C. Marcucci, D. Nyhan, and B. A. Simon, "Distribution of pulmonary ventilation using Xe-enhanced computed tomography in prone and supine dogs," *J. Appl. Physiol.*, vol. 90, no. 2, pp. 421–430, 2001.
[5] D. Chon, K. C. Beck, S. A. Simon, H. Shikata, O. I. Saba, and E. A. Hoffman, "Effect of low-xenon and krypton supplementation on signal/noise of regional CT-based ventilation measurements," *J. Appl. Physiol.*, vol. 102, no. 4, pp. 1535–1544, 2007.
[6] M. S. Albert, G. D. Cates, B. Driehuys, W. Happer, B. Saam, C. S. Springer, Jr., and A. Wishnia, "Biological magnetic resonance imaging using laser-polarized 129Xe," *Nature*, vol. 370, pp. 199–201, 1994.
[7] R. D. Black, H. L. Middleton, G. D. Cates, G. P. Cofer, B. Driehuys, W. Happer, L. W. Hedlund, G. A. Johnson, M. D. Shattuck, and J. C. Swartz, "In vivo He-3 MR images of guinea pig lungs," *Radiology*, vol. 199, no. 3, pp. 867–870, 1996.
[8] H. Middleton, R. D. Black, B. Saam, G. D. Cates, G. P. Cofer, R. Guenther, W. Happer, L. W. Hedlund, G. A. Johnson, K. Juvan, and J. Swartz, "MR imaging with hyperpolarized 3He gas," *Magn. Reson. Med.*, vol. 33, no. 2, pp. 271–275, 1995.
[9] E. van Beek, J. Wild, W. Schreiber, H. Kauczor, J. P. Mugler, III, and E. E. de Lange, "Functional MRI of the lungs using hyperpolarized 3-helium gas," *J. Magn. Reson. Imaging*, vol. 20, no. 4, pp. 540–554, 2004.
[10] E. A. Hoffman, B. A. Simon, and G. McLennan, "State of the art. A structural and functional assessment of the lung via multidetector-row computed tomography: Phenotyping chronic obstructive pulmonary disease," *Proc. Am. Thorac. Soc.*, vol. 3, pp. 519–532, 2006.
[11] E. A. Hoffman, J. M. Reinhardt, M. Sonka, B. A. Simon, J. Guo, O. Saba, D. Chon, S. Samrah, H. Shikata, J. Tschirren, K. Palagyi, K. C. Beck, and G. McLennan, "Characterization of the interstitial lung diseases via density-based and texture-based analysis of computed tomography images of lung structure and function," *Acad. Radiol.*, vol. 10, no. 10, pp. 1104–1118, 2003.
[12] E. A. Hoffman, D. Gnanaprakasam, K. B. Gupta, J. D. Hoford, S. D. Kugelmass, and R. S. Kulawiec, "VIDA: An environment for multidimensional image display and analysis," *Proc. SPIE*, vol. 1660, pp. 694–711, 1992.
[13] M. H. Tawhai, P. J. Hunter, J. Tschirren, J. Reinhardt, G. McLennan, and E. A. Hoffman, "CT-based geometry analysis and finite element models of the human and ovine bronchial tree," *J. Appl. Physiol.*, vol. 97, no. 6, pp. 2310–2321, 2004.
[14] M. H. Tawhai and P. J. Hunter, "Modeling water vapor and heat transfer in the normal and the intubated airway," *Ann. Biomed. Eng.*, vol. 32, no. 4, pp. 609–622, 2004.
[15] K. Burrowes and M. Tawhai, "Computational predictions of pulmonary blood flow gradients: Gravity versus structure," *Respir. Physiol. Neurobiol.*, vol. 154, no. 3, pp. 515–523, 2006.
[16] C.-L. Lin and E. A. Hoffman, "A numerical study of gas transport in human lung models," *Proc. SPIE*, vol. 5746, pp. 92–100, 2005.
[17] S. Kabilan, C.-L. Lin, and E. A. Hoffman, "Characteristics of air flow in a CT-based ovine lung: A numerical study," *J. Appl. Physiol.*, vol. 102, no. 4, pp. 1469–1482, 2007.
[18] C.-L. Lin, M. H. Tawhai, G. McLennan, and E. A. Hoffman, "Characteristics of the turbulent laryngeal jet and its effect on air flow in the human intra-thoracic airways," *Respir. Physiol. Neurobiol.*, vol. 157, no. 2–3, pp. 295–309, 2007.
[19] C.-L. Lin, H. Lee, T. Lee, and L. Weber, "A level set characteristic Galerkin finite element method for free surface flows," *Int. J. Numer. Methods Fluids*, vol. 49, no. 5, pp. 521–547, 2005.
[20] A. Vreman, "An eddy-viscosity subgrid-scale model for turbulent shear flow: Algebraic theory and applications," *Phys. Fluids*, vol. 16, no. 10, pp. 3670–3681, 2004.
[21] M. H. Tawhai, M. P. Nash, and E. A. Hoffman, "An imaging-based computational approach to model ventilation distribution and soft tissue deformation in the ovine lung," *Acad. Radiol.*, vol. 13, no. 1, pp. 113–120, 2006.
[22] J. W. Fernandez, P. Mithraratne, S. Thrupp, M. H. Tawhai, and P. J. Hunter, "Anatomically based geometric modelling of the musculo-skeletal system and other organs," *Biomech. Model. Mechanobiol.*, vol. 2, no. 3, pp. 139–155, 2004.
[23] G. Xia and C.-L. Lin, "An unstructured finite volume approach for structural dynamics in response to fluid motions," *Comput. Struct.*, vol. 86, no. 7–8, pp. 684–701, 2008.
[24] M. H. Tawhai and K. S. Burrowes, "Developing integrative computational models of pulmonary structure," *Anat. Rec. B New Anat.*, vol. 275, no. 1, pp. 207–218, 2003.
[25] F. S. Henry, J. P. Butler, and A. Tsuda, "Kinematically irreversible acinar flow: A departure from classical dispersive aerosol transport theories," *J. Appl. Physiol.*, vol. 92, no. 2, pp. 835–845, 2002.
[26] E. P. L. Roberts and M. R. Mackley, "The simulation of stretch rates for the quantitative prediction and mapping of mixing within a channel flow," *Chem. Eng. Sci.*, vol. 50, no. 23, pp. 3727–3746, 1995.